# $\beta$-chitosan-clay films: Characterization and antibacterial study using response surface methodology

Mohamed Hajjaji, Abdelhakim Alagui, Nicolas Joly, Patrick Martin

# β-chitosan-clays films: Characterization and antibacterial study using response surface methodology

| | |
|---|---|
| Journal: | *Polymers from Renewable Resources* |
| Manuscript ID | PRR-22-0014.R1 |
| Manuscript Type: | Original Article |
| Date Submitted by the Author: | n/a |
| Complete List of Authors: | Hajjaji, Mohamed; Cadi Ayyad University Faculty of Sciences Semlalia, Chemistry; University of Cadi Ayyad<br>Alagui, Abdelhakim; Cadi Ayyad University Faculty of Sciences Semlalia, Chemistry<br>Joly, Nicolas; Artois University, Unité Transformations & Agroressources<br>Martin, Patrick; Artois University, Unité Transformations & Agroressources |
| Keywords: | β-chitosan-clay films, structure, physical/mechanical properties, antibacterial activity, response surface methodology |
| Abstract: | Properties of the chitosan films can be improved by incorporating clay minerals. So, solvent-cast films of the β-chitosan containing stevensite-rich or kaolinitic-illitic clays (up to 50 mass %) were characterized for their structural and mechanical properties. The effects of molecular weight (MW) and deacetylation degree (DD) of chitosan, and the clay/chitosan mass ratio on the inhibition growth of Escherichia coli and Staphylococcus aureus were studied using the response surface methodology (RSM). The films consisted of exfoliated/intercalated or flocculated composites, and the electrostatic bonds formed between the functional moieties of the chitosan and the clay particles active sites essentially influenced their mechanical strength. The results of the study using RSM showed that the optimal value of MW required for the inhibition of the bacteria varied according to the film used, and high antibacterial activity necessitated high DD (89-97%). |
| | |

# β-chitosan-clays films: Characterization and antibacterial study using response surface methodology

Mohamed Hajjaji[1]*, Abdelhakim Alagui[1], Nicolas Joly[2], Patrick Martin[2]

[1]Laboratoire des Sciences des Matériaux et Optimisation des Procédés, Faculté des Sciences Semlalia, Université Cadi Ayyad, B.P. 2390, Av. Pce My Abdellah, Marrakech 40001, Morocco.
[2] Unité Transformations & Agroressources- ULR7519, Univ. Artois, UniLasalle, F-62408 Béthune, France.

## Abstract

Properties of the chitosan films can be improved by incorporating clay minerals. So, solvent-cast films of the β-chitosan containing stevensite-rich or kaolinitic-illitic clays (up to 50 mass %) were characterized for their structural and mechanical properties. The effects of molecular weight (MW) and deacetylation degree (DD) of chitosan, and the clay/chitosan mass ratio on the inhibition growth of *Escherichia coli* and *Staphylococcus aureus* were studied using the response surface methodology (RSM). The films consisted of exfoliated/intercalated or flocculated composites, and the electrostatic bonds formed between the functional moieties of the chitosan and the clay particles active sites essentially influenced their mechanical strength. The results of the study using RSM showed that the optimal value of MW required for the inhibition of the bacteria varied according to the film used, and high antibacterial activity necessitated high DD (89-97%).

**Keywords:** β-chitosan-clay films, structure, physical/mechanical properties, antibacterial activity, response surface methodology

*Correspondence: hajjaji@uca.ma

## 1. Introduction

Chitosan is a deacetylated derivative of the chitin, which is a constituent of shellfish and crustaceans exoskeletons, among others. It is a copolymer composed of β-(1-4)-2-amino-D-glucose and β-(1-4)-2-acetamido-D-glucose units. Three polymorphic forms (α, β and γ) of chitosan are identified. β-chitosan is more soluble and more reactive than α-chitosan,[1] which is the most abundant form. Chitosan is suitable for many practical uses[2-6] because of its non-toxicity, biodegradability, film-forming character, and high density of positive charges associated with the protonated amino-groups. The chitosan exhibited a good antibacterial activity. Referring to some authors, the antibacterial activity of β-chitosan was higher than that of α-chitosan.[1]

The inhibition processes depend on chitosan characteristics, mainly its deacetylation degree (DD) and molecular weight (MW), as well as on bacteria strain.[7-9] It can be summarized that the higher the DD, the better the inhibition. This fact is linked to the abundance of protonated amino-groups, and to their ability to interact with the specific functional groups of cells membrane macromolecules.[10] The studies dealing with the influence of MW on the inhibition of bacteria growth, such as *Escherichia coli*, showed different results.[10] Disparate effects of MW on chitosan antibacterial properties were cited elsewhere.[11] According to Raoka et al.[12] the effect of MW on the antibacterial activity of chitosan is greater than that of DD.

Clay minerals, especially those of the smectite group, can be delaminated. So, nano-sized particles with high-aspect ratio are obtained. Compared to kaolinite and illite, smectite minerals have high cation exchange capacity (CEC) and surface area.[13] Owing to these characteristics and to their anionic character, these clay minerals are suitable materials for medical and cosmetic purposes.[14]

To improve mechanical and barrier properties of chitosan films for drug carrying and food packaging uses, the chitosan was mixed with limited amounts (up to about 5 wt%) of montmorillonite.[15-17] The addition of the montmorillonite (di-octahedral clay mineral of the smectite group) to chitosan resulted in the formation of nanocomposites with efficient bactericidal effects.[16, 18, 19] So far, no attention has been paid to the study of antibacterial activity of β-chitosan films containing stevensite or kaolinitic-illitic clays. Stevensite is a tri-octahedral swelling clay mineral, which belongs to the smectite group such as montmorillonite. So, chitosan association with limited amount of stevensite should result in intercalated and/or exfoliated nanocomposites formation. The lack of studies related to bacterial inhibition by chitosan-stevensite films could be due to stevensite scarcity. Kaolinite

and illite are non-expandable natural clay minerals,[13] and chitosan intercalation in the interlayer spaces of their pristine structures could not occur. Thereby, chitosan association with kaolinite or illite should lead to tactoids formation. In such a condition, kaolinite as well as illite behaves like conventional fillers. To obtain chitosan-kaolinite nanocomposites films, some authors prepared exfoliated kaolinite by mechano-chemical treatment.[20]

The use of β-chitosan-montmorillonite films as bactericidal materials has been ignored in spite of the potential reactivity of β-chitosan, which consists of parallel chains with weak intermolecular bonds.[21] For the same amount of montmorillonite (up to 5 mass%), β chitosan-based films showed higher tensile strength and Young's modulus than those of α chitosan-based films, and both films manifested similar water solubility.[22]

The influences of chitosan characteristic (DD and MW) and clay/chitosan ratio changes on the inhibition of pathogenic bacteria growth have not been investigated, probably because of the numerous experiences required. This drawback could be overcome by using the response surface methodology.[23]

In this study, the structure of solvent-casted films composed of β-chitosan and stevensite-rich clay (RH) or kaolinitic-illitic clay (BN2) was examined. Moreover, the changes of the physical/mechanical properties of films according to clay additions were followed. In addition, the growth inhibition of the most prevalent bacteria (*Escherichia coli* and *Staphylococcus aureus*) according to chitosan DD, chitosan MW, and clay/chitosan ratio was assessed using the RSM.

## 2. Materials and Methods

### 2.1. β-chitosan

The β-chitosan was prepared from the chitin, extracted from the pens of local squid. For this purpose, finely ground squid pens were demineralized with HCl solution (0.55 N) and deproteinized with heated NaOH solution (80 °C, 0.33 N). The pens powder/solution ratio was 1:10 (w/v). To prepare chitosan, chitin was deacetylated for 24 h using NaOH solution (40 mass%) and standard reflux setup.[24] The X-ray diffraction pattern of the prepared chitosan is shown in Fig.1. Taking into consideration the latter trace, and using the Scherrer's equation and the crystallinity index determination method given in Focher et al.,[25] the chitosan crystallinity index and apparent crystal size were found to be 77 and 2.1 nm, respectively.

Referring to the thermal curve shown in Fig. 2, the chitosan was thermally stable up to about 266°C.

The molecular weight (MW) of the chitosan was calculated using the Mark-Houwink equation.[26]

$$[\eta] = K(MW)^a \qquad (1)$$

η is the intrinsic viscosity, K and a are determined constants. The deacetylation degree (DD) of the chitosan was determined by potentiometric titration following the experimental procedure in Tolaimate et al.[24], and using the following equation.[27]

$$DD = \frac{203(V_2 - V_1)N}{m + 42(V_2 - V_1)N}$$

$V_1$ and $V_2$ are the volumes of NaOH solution at the first and the second neutralization points. N is the strength of the alkali solution used. m is the weight of the chitosan sample.

## 2.2. Clays

Clays, referenced as RH and BN2, were taken from clay pits located at Jbel Rhassoul (Midelt province, Morocco) and Tetouan-Hoceima province (Morocco), respectively. They consisted of stevensite and an assemblage of kaolinite and illite, respectively. Quartz and carbonates were the main ancillary minerals found. The chemical compositions of RH and BN2 are given in Table 1, and their cation exchange capacities, determined by the cobaltihexamine chloride method[28] were 0.8 and 0.3 meq/g, respectively. The decarbonation of clays was done with a buffer acetic acid/Na-acetate solution (pH = 4.74). The carbonate-free clays (particles size < 80 µm) were sodium-saturated,[24] and oven dried at 105 °C.

## 2.3. Chitosan-clay films

Chitosan-clay films (clay/chitosan mass ratio ≤ 100%) were prepared with the solvent casting technique.[30] For this purpose, sample (≤ 1 g) of the sodium-saturated clay was dispersed in 5 mL of acetic acid (1% v/v) solution, and stirred for 24 h. On the other hand, a portion of chitosan (1 g) was introduced in 100 mL of an acetic acid solution (1 %v/v), and stirred for 2 h. The limpid solution of chitosan was mixed with the clay dispersion, and the mixture was homogenized for 24 h. 25 mL of the mixture was poured in a Petri dish and kept at 30°C for 48 h, so to evaporate water. The film formed was retrieved and soaked with a solution of NaOH (0.5 M) for 12 h, rinsed with distilled water, and dried at 25 °C. The thickness of the films was of about 10 µm.

### 2.4. Physical/mechanical properties of the film

The mass loss of films was determined by weighing disks (~3 cm diameter) before and after immersion in 50 mL of distilled water stirred at 350 rpm for 24 h. The tensile strength and the elongation at break of films were measured on strips according to the ASTM D882,[31] using an Instron universal machine operating with a crosshead speed of 50 mm/min. The measurements were done in triplicate.

### 2.5. Analysis techniques

Fourier-transform infrared (FT-IR) analyses were carried out on thin disks composed of 1mg sample and 99 mg KBr. The spectra were recorded with a Perkin Elmer 1725 spectrophotometer functioning in the range of 4000–400 $cm^{-1}$ at a resolution of 4 $cm^{-1}$. The X-ray diffraction (XRD) analyses were performed on powder samples with a Philips X'Pert MPD diffractometer operating with a copper anode ($\lambda_{K\alpha}$ = 1.5418 Å). The step size (°2θ) and the scan step time were set at 0.013 and 1 s, respectively.

### 2.6. Percentage inhibition of bacteria growth

To determine the percentage inhibition (PI) of bacteria growth, a bacteria suspension (considered as a blank suspension) was adjusted to $10^5$-$10^6$ CFU/mL using sterile saline water (0.9% w/v). A film sample (9 $cm^2$) was introduced in a tube containing 5 mL of nutrient broth, and autoclaved at 120 °C for 20 min. Then, the tube was inoculated with 0.5 mL of the bacteria suspension, and incubated at 37 °C for 24 h. The optical density (OD) of the incubated and the blank suspensions were measured by using an UV-visible spectrophotometer operating at 620 nm.[32] These data were used to calculate PI:

$$\mathbf{PI}\ (\%) = \frac{\mathbf{OD\ of\ the\ blank\ suspension - OD\ of\ the\ incubated\ \ suspension}}{\mathbf{OD\ of\ the\ blank\ suspension}}\ \mathbf{x\ 100} \qquad (2)$$

### 2.7. Effects of the chitosan characteristics and the clay/chitosan ratio on the growth inhibition of the bacteria

The weights of the effects of clay/chitosan mass ratio (R), DD and MW on the PI of bacteria were assessed using the RSM and adopting the following model:[33]

$$\boldsymbol{Y = b_o + \sum_{i=1}^{3} b_i X_i + \sum_{i=1}^{3} b_{ii} X_{ii}^2 + \sum_{1 \le i < j}^{3} b_{ij} X_i X_j} \qquad (3)$$

Where Y = PI, and $b_o$, $b_i$, $b_{ii}$ and $b_{ij}$ are constant. $X_1$, $X_2$ and $X_3$ are the coded variables: $X_1 = (R\text{-}R_o)/\Delta R$, $X_2 = DD\text{-}(DD)_o/\Delta(DD)$ and $X_3 = MW\text{-}(MW)_o/\Delta(MW)$. Considering the

factors domains investigated: $0 \leq R \leq 100\%$, $70 \leq DD \leq 100\%$, $50000 \leq MW \leq 400000$ g/mol, the factors values at the centers of these domains, and the variation steps were: $R_o = 0.5$, $(DD)_o = 85$ %, $(MW)_o = 225000$ g/mol, and $\Delta R = 0.5$, $\Delta(DD) = 15$ %, $\Delta(MW) = 175000$ g/mol. The Doehlert design and the least-square regression method were adopted for the determination of the constants.[34,35] The experiments planned according to the Doehlert design and the PI measured ($Y_1$, $Y_2$) are given in Table 2.

The validity of the polynomial models was assessed on the basis of the analysis of variance (ANOVA) and checked by the probability plot of residuals.

## 3. Results and discussion

### 3.1. Structural characterization of the chitosan-clay films

As can be deduced from the typical XRD patterns shown in Fig. 3A, the association of β-chitosan with BN2 clay did not have impact on the position of the basal reflexions of illite (°2θ = 8.78) and kaolinite (°2θ = 12.48). So, the interlayer space of both clay minerals remained unchanged, and consequently intercalated composites did not occur in this case. So, tactoid structure took place.[36] Considering that the points of zero charge of chitosan and chitosan-clay films (Table 1) were somewhat similar, the surface charge densities of these materials were comparable. So, BN2 particles were layered with chitosan.

Referring to Fig. 3B, the basal X-ray reflexion of the stevensite (°2θ = 6.02) vanished as a result of the association of RH clay with β-chitosan. This fact was associated to stevensite delamination caused by excessive expansion of the interlayer due to the excessive insertion of chitosan chains. Such a phenomenon was also observed in the case of mixing montmorillonite (smectite clay mineral) with chitosan.[37] Stevensite particles, as was the case with BN2 particles, were coated with chitosan because the $pH_{PZC}$ of stevensite-containing films and chitosan were close (Table 1). However, in this case exfoliated/intercalated structure was formed.

Considering the FT-IR analyses shown in Fig. 4A, the spectrum of the film (b) consisted of an additional band at 1566 $cm^{-1}$, which is associated to the protonated amino-groups of chitosan. In addition, the band at 1417 $cm^{-1}$, which is attributed to the deformation of the $CH_2$ in the $CH_2OH$ group of the chitosan, intensified. The bands related to the clay minerals bonds were not modified. These results allowed the deduction that the functional

groups ($-NH_3^+$ and $CH_2OH$) of the chitosan were involved in its retention by clay particles surfaces, which are negatively charged.

The comparative examination of FT-IR spectra given in Fig. 4B showed that the band at 1420 $cm^{-1}$associated to the $CH_2$ in the $CH_2OH$ group of the chitosan was well distinguished on the spectrum of the film (b), whereas the remaining bands were not affected. So, it was believed that the primary hydroxyl group of chitosan developed hydrogen bonds with stevensite particles, known as anionic clay mineral. These bonds played a key role in the adsorption of the chitosan on the clay particles.

SEM examinations of chitosan-BN2 films showed clay aggregates such as seen in Fig. 5A (micrograph a) together with embedded particles (Fig. 5A, micrograph b). In addition, chitosan-rich zones were identified (Zone 1). These observations allowed the deduction that chitosan-BN2 films consisted of segregated domains and the inter-aggregates spaces were chitosan-rich zones. The SEM observations realized on chitosan-RH films revealed scarce clay aggregates (Fig. 5B, micrograph b), and chitosan-coated clay particles such as shown in Fig. 5B (micrograph b). The scarcity of clay aggregates was associated to the clay exfoliation and the formation of exfoliated/intercalated composites, as previously mentioned. .

### 3.2. Physical/mechanical properties and thermal stability of the films

#### 3.2.1. Films mass loss

The mass loss of films containing up to about 0.15 g of RH/g of chitosan was somewhat constant (3.5 ± 0.7 mass%) (Fig. 6, curve a). However, it increased almost linearly with the increase of clay content, and the increment was of 10.3xMc (Mc : mass of the clay added). Considering chitosan and clay characteristics (DD = 90%, CEC (cation exchange capacity) = 0.8 meq/g), the estimated amount of glucosamine unit per one gram of β-chitosan was of $5.56x10^{-3}$ mole, and the quantity of clay active sites was of $8x10^{-4}$ mol/g. Hence, the portion of chitosan bonded to RH particles (0.15 g) was not significant (~ 2%), and the clay particles were thick-coated with chitosan. In the clay-rich films, a portion of clay particles was scarcely coated with chitosan. So, in such a condition, the clay particles were easily lost.

The mass loss of chitosan-BN2 films, which consisted of up to 0.5 g BN2 per g chitosan, was almost constant (Fig. 6, curve b). However, it increased linearly in the case of clay-rich films. In this case, the mass loss per gram of clay was estimated to be 10.5.

Taking into consideration the DD of chitosan and the CEC of BN2 clay (0.3 meq/ g), together with the fact that the hydroxyls of chitosan were implicated in the association of film

constituents, the fraction of chitosan involved in the binding process was estimated to be 10% for the film containing 0.5 g BN2. Thus, a high amount of chitosan was stacked over the clay particles, and flocculated composite formed.

In view of the above results, the abundance of flocculated composites in chitosan-clay films contributed to the reduction of clay particles loss.

### 3.2.2. Thermal stability of the films

The thermal curves of chitosan-BN2 and chitosan-RH films displayed endothermic peaks at 89 and 92°C, and exothermic effects at 277 and 280°C, respectively (Fig. 2). The endotherms were associated to the loss of physisorbed water. The exotherms were assigned to the chitosan decomposition. The relative thermal stability shown by clay-containing films could be associated to the clay characteristics (nanosized structure, high aspect ratio) and to their barrier effect.[38]

### 3.2.3. Mechanical properties

Small additions of RH (< ~0.14 g/g chitosan, i.e. 12 mass%) to β-chitosan improved the Young's modulus as well as the tensile strength of films (Fig. 7A), but they led to the reduction of the elongation at break and the tensile energy absorption (Fig. 7B). Excessive additions (> 20 wt %) resulted in the decline of the films stiffness.

The tensile strength of the chitosan-BN2 films containing up to about 0.25 g clay /g chitosan increased with respect to that of the chitosan film (Fig. 8A), whereas the Young's modulus (Fig. 8A), the elongation at break and the tensile energy absorption (Fig. 8B) fluctuated. For clay-rich films, the mechanical properties declined for the reasons given below.

In overall, the mechanical properties of polymer-based composites are affected by the inherent characteristics of the components used, the amount and the distribution of fillers, the interfacial bonding as well as by the processing methods.[39] Considering chitosan-RH films, the improvement of films mechanical resistance was essentially due to the formation of hydrogen bonds between the chitosan and the delaminated clay particles. In fact, the formation of tough interfaces clay/chitosan facilitated the load transfer across the film, and consequently the stress was homogeneously distributed.[40] However, as the volume fraction of RH exceeded 1.6% (v/v), the clay addition had a detrimental effect on film mechanical resistance. It was believed that because of the swelling character of RH clay, the clay-rich films were the object of microcraks due to the drying shrinkage. The formation of such

defects together with the uneven distribution of the clay particles could be responsible for the decline of mechanical strength.

For BN2-containing films, the presence of the aforementioned electrostatic forces seemed to play a main role in the improvement of mechanical resistance of films with clay fraction < 3.2% (v/v). Further clay additions resulted in a drop of mechanical strength, possibly because of the flocculation and/or the heterogeneous distribution of clay particles.

### 3.3. Kinetics of the growth inhibition of the bacteria

Referring to the kinetics curves given in Fig. 9A, PI of the *E. coli* growth by the films approximated 90 to 100% after 24 h. The kinetics of the inhibition of the bacteria growth followed the pseudo-first order equation:

$$(PI)_t = (PI)_e e^{-kt} \qquad (4)$$

$(PI)_t$ and $(PI)_e$ are the instantaneous and the equilibrium percentages inhibition of the *E. coli* growth, respectively, k and t are the rate constant and time. The estimated values of k were of $3.12 \times 10^{-5}$ $s^{-1}$ and $3.45 \times 10^{-5}$ $s^{-1}$ for RH- and BN2- containing films, respectively. Based on the linear evolution of $PI = f(\sqrt{time})$ curves, the kinetics of the inhibition process was chiefly controlled by the diffusion process,[41] which seemed to be affected by the closest environment of cells (boundary layer). The diffusion process likely represented the leakage of vital intracellular substances, as the interaction between the chitosan and the negatively charged phospholipid bilayer of the bacterium has a detrimental effect on membrane permeability.[10,18,19]

Taking into consideration the curves shown in Fig. 9B, the kinetics of the inhibition of the *S. aureus* growth by the RH-chitosan film was relatively slow, but for both films, the change of the PI versus time fitted better the following linear form of the pseudo-second kinetics equation:

$$\frac{t}{(PI)_t} = \frac{t}{(PI)_e} + \frac{1}{k_2 (PI)_e^2} \qquad (5)$$

$k_2$ is the rate constant. $(PI)_t$, $(PI)_e$ and t kept the same meaning. The values of $k_2$ were determined to be $3.17 \times 10^{-2}$ and $5.88 \times 10^{-2}$ /s.(%) for RH- and the BN2-based films, respectively.

In view of the above results, the kinetics of inhibition process was mainly dependent on the interaction between microorganisms and film constituents, mainly chitosan. Indeed, according to some authors,[10] the lipoteichoic acid, which is a constituent of the cell wall of the

gram-positive bacteria, such as the *S. aureus*, can interact with chitosan, and results in the disturbance of the cell membrane functions. The built up of chitosan around the cell wall might impede the entrance of nutriments and the release of residue by the cell. Therefore, cell metabolism was drastically altered. On the other hand, the PI of the *E. coli* was controlled by diffusion, seemingly owing to the loss of the selective permeability of the cell membrane. This fact was attributed to the interaction between the anionic groups of bacterial membrane lipopolysaccharide and the protonated amino-groups of chitosan.[10]

### 3.4. Evaluation of the effects of the factors studied on the bacteria inhibition

The ANOVA results (Table 3) showed that the F-ratio was somewhat high and the statistical significance was smaller than 0.05, which is considered as the maximum limit to assert the validity of the proposed model.[42] So, the variations of PI (Yi) of the bacteria by both films as a function of the coded variables related to R, DD and MW were adequately described by the following equations:

$Y_1$ (Chitosan-RH/*E. coli*) = $45.3+5.0\ X_1+27.7\ X_2-21.2\ X_3+36.5\ X_1X_2-34.7X_1X_3-50.2X_2X_3-40.6\ X_1^2-25.8X_2^2-15.6X_3^2$ (6)

$Y_2$ (Chitosan-RH/*S. aureus*)= $43.8-1.0\ X_1+28.4\ X_2-21.3\ X_3+53.6\ X_1X_2-22.5X_1X_3-61.0X_2X_3-29.0X_1^2-10.4X_2^2-29.8X_3^2$ (7)

$Y_1$ (Chitosan-BN2/*E. coli*) = $95.2-42.9X_1+27.6X_2+13.7\ X_3-35.7X_1X_2-53.8X_1X_3+7.6X_2X_3-45.5X_1^2-66.8X_2^2-62.2X_3^2$ (8)

$Y_2$ (Chitosan-BN2/*S. aureus*) = $97.2-6.4X_1+39.2X_2+57.1X_3-5.1X_1X_2-2.0X_1X_3-18.5X_2X_3-9.8X_1^2-65.0X_2^2-54.2X_3^2$ (9)

The validity of these models was also assessed by the probability plot of residuals.[35] The almost linear distribution of the residuals, shown in Fig. 10, supported the adequacy of these polynomial models.

The comparison of the algebraic values of the linear terms $b_2X_2$ (equations 6-9) pointed out that the increase of DD, which is correlated to the increase of the chitosan amino-groups amount, improved the inhibition growth of both strains of bacteria. This result was in conformity with the above discussion that is the amino-groups were the main functional moieties involved in the inhibition of the bacteria growth. Considering the linear terms of the equations 6 and 7, the weights of the studied factors effects on PI followed the order: DD > MW > R. Moreover, PI using chitosan-RH films decreased with the increase of MW. In contrast, it increased with the use of chitosan-BN2 films (equations 8 and 9). These results supported the disparate effects of MW on the bactericidal activity.[10] Recalling the above

equations, the weight of the effect of R on PI was relatively low, except in the case of the equation 8 where the increase of R resulted in the decline of PI.

Taking into consideration the $b_{ij}X_iX_j$ terms of the equations 6, 7 and 9, the most important influencing interaction was that occurring between DD and MW. This interaction was categorized as an antagonistic one because the simultaneous rise of DD and the decrease of MW or vice-versa should result in the increase of PI. A typical response surface representing the antagonistic effect of the interaction between DD and MW is shown in Fig. 11a. In the case of the equation 8, R and MW interacted antagonistically and their interaction had the prominent effect on PI. The response surface showing the variation of PI against R and MW is given in Fig. 11b.

The optimal operating factors for high inhibition of the bacteria growth, which were determined by using the desirability function approach, are given in Table 4. Based on these results, the films composed of chitosan with high DD should inhibit the growth of both bacteria strains, as previously documented. In addition, the films consisting of about 40 mass% RH of chitosan with low to moderate MW should be highly effective against the tested bacteria. In the case of the chitosan-BN2 films, the use of chitosan with high MW is one of the operating conditions for high inhibition of the bacteria growth.

Considering the PI = f(clay/chitosan) curves plotted on the basis of the equations 6-9 (Fig. 12), the antibacterial effect of the chitosan film was less important as compared to that of the chitosan-RH films, which consisted of exfoliated/intercalated composites. In contrast, it was almost equivalent or somewhat better than that of the chitosan-BN2 films, which were composed of tactoids.

## 4. Conclusions

Stevensite-containing chitosan films consisted of exfoliated/intercalated nanocomposites, and the association between the films components were presumably achieved through hydrogen bonding. Limited additions of RH (up to 0.14 g /g chitosan) improved films tensile strength and Young's modulus, but they had a negative impact on their elongation at break.

Chitosan films containing kaolinitic-illitic clay were essentially composed of flocculated composites. The amino-groups together with the hydroxyls of chitosan were involved in its association with the clay particles. The addition of BN2 clay (up to 0.25 g BN2/g chitosan) improved the mechanical strength of films.

The results of the kinetics of the bacteria growth inhibition by the studied films allowed the deduction that the inhibition process depended on the bacterial strain. In the case of *E. coli*, the cell membrane seemed to be damaged due to its interaction with the protonated amino-groups of chitosan, and the vital substances flowed out. For *S. aureus*, the nutrients seemed to be impeded to get into the cells because of the stack of chitosan over their membranes.

The polynomial models obtained by using the RSM allowed the prediction of the effects of the factors studied and of their mutual interactions on PI. The rise of MW resulted in the decrease of the PI of *E. coli*, but it increased that of the *S. aureus*. The increase of DD yielded to the rise of PI, and the optimal value should be in the range of 89-97%. Based on the RSM results, the antibacterial activity of the chitosan film was a good as that of the tactoid-rich films. However, it was less significant as compared to that of the films composed of exfoliated/interacted clay.



## Acknowledgement

This work was supported by the CNRST (grant number PPR/26/2015).

## References

1. Van Hoa N, Vuong NTH, Minh NC, et al. Squid pen chitosan nanoparticles: small size and high antibacterial activity. *Polymer Bulletin* 2021; 78: 7313–7324.
2. Choi C, Nam JP and Nah JW. Application of chitosan and chitosan derivatives as biomaterials. *J Ind Eng Chem* 2016; *33:* 1–10.
3. Dutta PK, Dutta J and Tripathi VS. Chitin and chitosan: Chemistry, properties and applications. *J Sci Ind Res* 2004; 63: 20-31.
4. Islam S, Rahman Bhuiyan MA and Islam MN. Chitin and chitosan: Structure, properties and applications in biomedical engineering. *J Polym Environ* 2017; 25: 854–866.
5. Mahmoud MG, El Kady E and Asker, MS. Chitin, chitosan and glucan, properties and applications. *World J. Agri. Soil. Sci.* 2019; 3(1). DOI: 10.33552/wjass.2019.03.000553.

6. Rinaudo M. Chitin and chitosan: properties and applications. *Prog Polym Sci* 2006; 31: 603–632.

7. Walke S, Srivastava G, Nikalje M, et al. Physicochemical and functional characterization of chitosan prepared from shrimp shells and investigation of its antibacterial, antioxidant and tetanus toxoid entrapment efficiency. *Int J Pharm Sci Rev Res* 2014; 26(2): 215-225.

8. Wang W, Xue C and Mao X. Chitosan: Structural modification, biological activity and application. *Int J Biol Macromol* 2020; 164: 4532–4546.

9. Confederat LG, Tuchilus CG, Dragan M, et al. Preparation and antimicrobial activity of chitosan and its derivatives: A concise review, *Molecules* 2021; 26: 3694.

10. Kong M, Chen XG, Xing K, et al. Antimicrobial properties of chitosan and mode of action: A state of the art review. *Int J Food Microbiol* 2010; 144: 51–63.

11. Li J and Zhuang S. Antibacterial activity of chitosan and its derivatives and their interaction mechanism with bacteria: Current state and perspectives. *Eur Polym J* 2020; 138: 109984. DOI: 10.1016/j.eurpolymj.2020.109984.

12. Rajoka MSR, Mehwish HM, Wu Y, et al. Chitin/chitosan derivatives and their interactions with microorganisms: a comprehensive review and future perspectives. *Critical Reviews in Biotechnology* 2020; 40(3): 365-379.

13. Murray HH. Applied clay mineralogy-occurrences, processing and applications of kaolins, bentonites, palygorskite-sepiolite, and common clays, Development in clay science 2, Elsevier, 2007.

14. Carretero MI and Lagaly G. Clays and health: An introduction. *Appl Clay Sci* 2007; 36: 1–3.

15. De Azeredo HMC. Nanocomposites for food packaging applications. *J Int Food Res* 2009; 42: 1240–1253.

16. Han Y-Su, Lee S-H, Choi KH, et al. Preparation and characterization of chitosan–clay nanocomposites with antimicrobial activity. *J Phys Chem Solids* 2010; 71: 464–467.

17. Qu B and Luo Y. A review on the preparation and characterization of chitosan-clay nanocomposite films and coatings for food packaging applications. *Carbohydrate Polymer Technologies and Applications* 2021; 2: 100102. DOI: 10.1016/j.carpta.2021.100102.

18. Chandrasekaran M, Kim KD and Chun SC. Antibacterial activity of chitosan nanoparticles: A Review. *Processes* 2020; 8: 1173. DOI:10.3390/pr8091173.

19. Kassem A, Ayoub GM and Malaeb, L. Antibacterial activity of chitosan nano-composites and carbon nanotubes: A review. *Sci Total Environ* 2019; 668: 566–576.

20. Neji AB, Jridi M, kchaou H, et al. Preparation, characterization, mechanical and barrier properties investigation of chitosan-kaolinite nanocomposites. *Polymer Testing* 2020; 84: 106380. DOI: 10.1016/j.polymertesting. 2020.106380.

21. Kurita K, Tomita K, Tada T, et al. Squid chitin as a potential alternative chitin source: Deacetylation behavior and characteristic properties. *J Polym Sci Part A-1: Polym Chem* 1993; 31: 485-491.

22. Mourak A, Hajjaji M, Alagui A, et al. Effects of geomaterial-originated fillers on microstructure and mechanical/physical properties of α- and β-chitosan-based films. *Molecules* 2021; 26: 7514. DOI: 10.3390/molecules26247514.

23. Khalfaoui A, Hajjaji M, Kacim S, et al. Evaluation of the simultaneous effects of firing cycle parameters on technological properties and ceramic suitability of a raw clay using the response surface methodology. *J Am Ceram Soc* 2006; 89 (5): 1563–1567.

24. Tolaimate A, Desbrières J, Rhazi M, et al. A. Contribution to the preparation of chitins and chitosans with controlled physicochemical properties. *Polymer* 2003; 44: 7939–7952.

25. Focher B, Beltranme PL, Naggi A, et al. Alkaline N-deacetylation of chitin enhanced by flash treatments. Reaction kinetics and structure modifications. *Carbohydr Polym* 1990; 12: 405–418.

26. Maghami GG and Roberts GAF. Evaluation of the viscometric constants for chitosan. *Makromol. Chem.* 1988; 189: 195-200.

27. Gupta KC and Jabrail FH. Effects of degree of deacetylation and cross-linking on physical characteristics, swelling and release behavior of chitosan microspheres. *Carbohydrate Polymers* 2006; 66: 43–54.

28. Aran D, Maul A and Masfaraud J-F. A spectrophotometric measurement of soil cation exchange capacity based on cobaltihexamine chloride absorbance. *C. R. Geoscience* 2008 ; 340 : 865–871.

29. Lagaly G. Colloid clay science. In: Bergaya, F.; Theng, BKG.; and Legally, G.(eds) Handbook of Clay Science-Developments in Clay Science. Elsevier, 2006, p.141.
30. Tang ZG, Black RA, Curran JM, et al. Surface properties and biocompatibility of solvent-cast poly[e-caprolactone] films. *Biomaterials* 2004; 25: 4741–4748.
31. ASTM D882-18.Standard Test Method for Tensile Properties of Thin Plastic Sheeting; ASTM International: West Conshohocken, PA, USA, 2018.
32. Muloiwa M, Nyende-Byakika S and Dinka M. Comparison of unstructured kinetic bacterial growth models. *S Afr J Chem Eng* 2020; 33: 141–150.
33. El Hafid K, and Hajjaji M. Geopolymerization of glass- and silicate-containing heated clay. *Constr Build Mater* 2018; 159: 598–609.
34. Ferreira SLC, dos Santos WNL, Quintella CM,et al. Doehlert matrix: a chemometric tool for analytical chemistry-review. *Talanta* 2004 ; 63 : 1061–1067.
35. Mathieu D. Phan Tan Luu, R. Software NEMROD. Université d'Aix, Marseille III, France, 1980.
36. Qu B and Luo Y. A review on the preparation and characterization of chitosan-clay nanocomposite films and coatings for food packaging applications. *Carbohydrate Polymer Technologies and Applications* 2021; 2: 100102.
37. Darder M, Colilla M and Eduardo Ruiz-Hitzky E. Biopolymer−clay nanocomposites based on chitosan intercalated in montmorillonite. *Chem Mater* 2003; 15: 3774–3780.
38. Leszczynska A, Njuguna J, Pielichowski K, et al. Polymer/montmorillonite nanocomposites with improved thermal properties. Part II: Thermal stability of montmorillonite nanocomposites based on different polymeric matrixes. *Thermochim. Acta* 2007; 454 : 1–22.
39. Tjong SC. Structural and mechanical properties of polymer nanocomposites. *Mater Sci Eng R Rep* 2006; 53: 73–197.
40. Rhim JW, Hong SI, Park HM, et al. Preparation and characterization of chitosan-based nanocomposite films with antimicrobial activity. *J Agric Food Chem* 2006; 54: 5814-5822.
41. Ismadji S, Edi Soetaredjo F and Aning Ayucitra A. Clay materials for environmental remediation. Springer, 2015, p.113.

42. Myers RH, Montgomery DC and Anderson-Cook CM. Response surface methodology: process and product optimization using designed experiments, 4th Edition Joh.

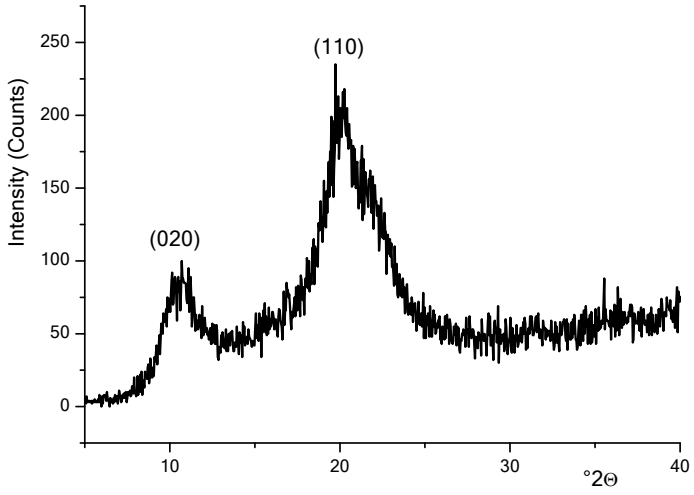


**Figure 1.** X-ray diffraction trace of the prepared chitosan.

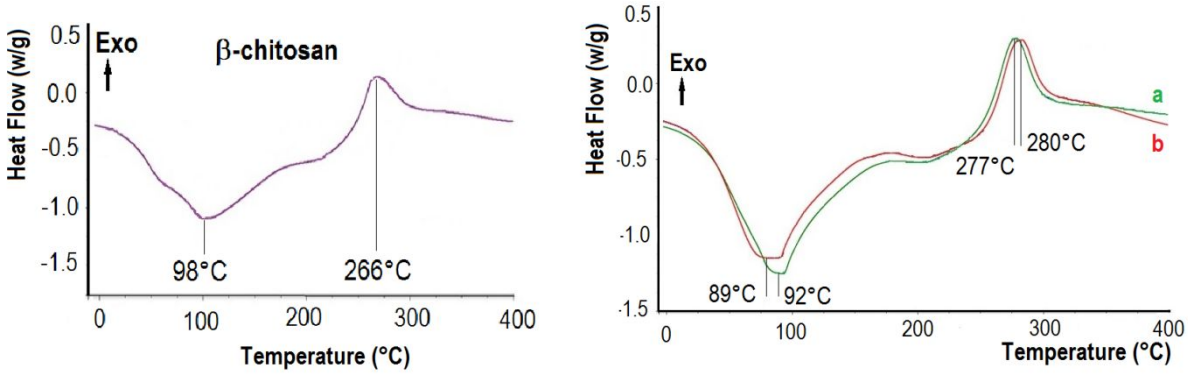


**Figure 2.** Thermal curves of the prepared chitosan, BN2- chitosan (a) and RH-chitosan (b) films. (clay/chitosan mass ratio: 0.25/1).

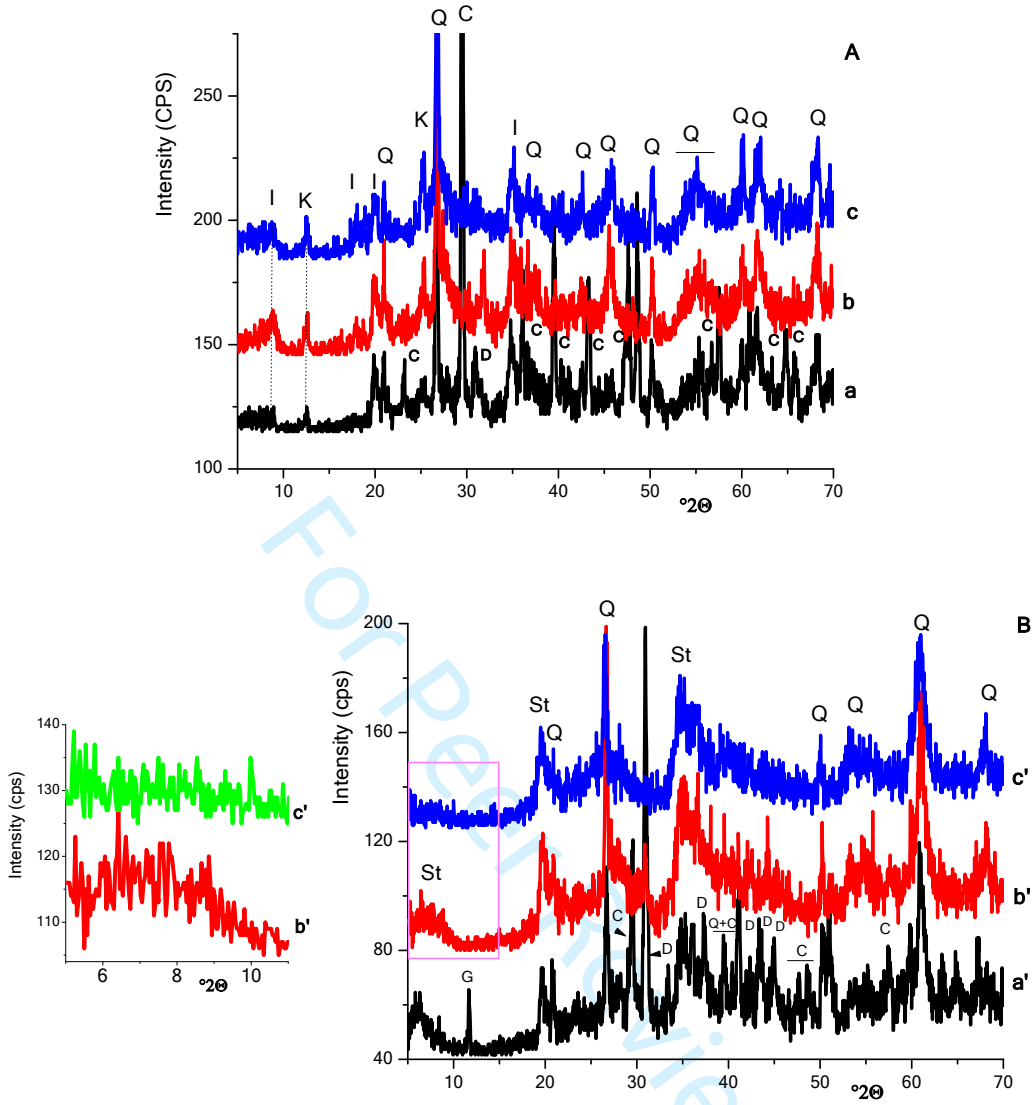


**Figure 3.** XRD patterns of the clays (**a, a'**), the sodium-loaded clay fractions (**b, b'**) and the chitosan-clay films (**c, c'**). (**A**) and (**B**) are associated to BN2 and RH, respectively. I: illite, K: kaolinite, Q: quartz, C: calcite, D: dolomite, St: stevensite, G: gypsum. (clay/chitosan mass ratio: 1/1).

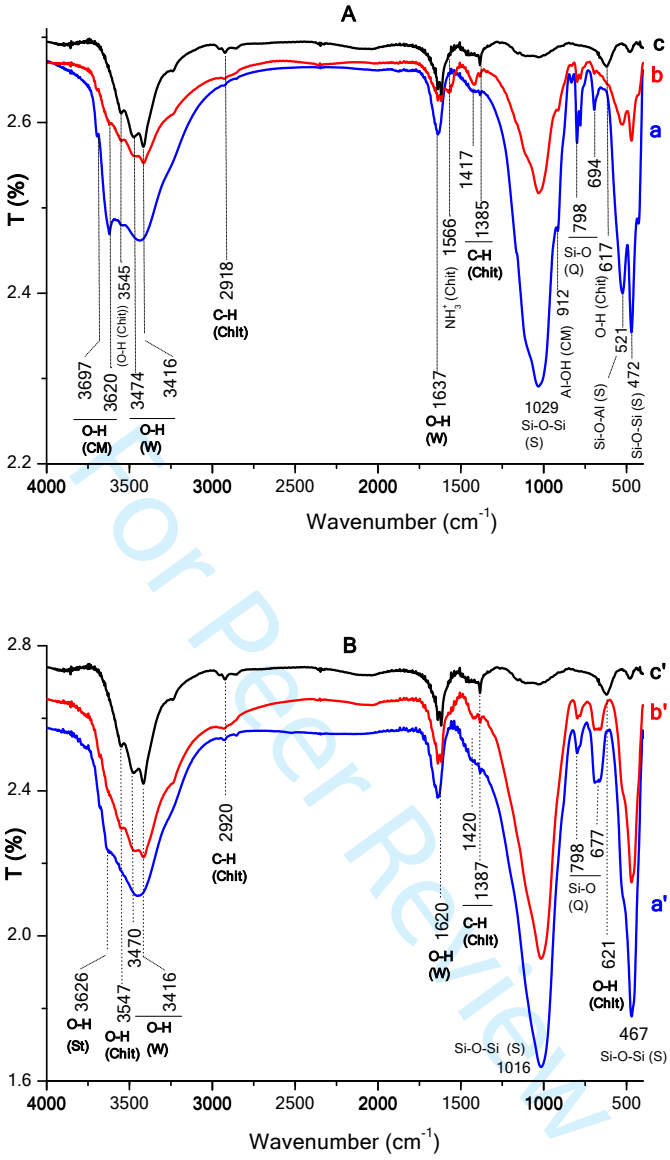


**Figure 4.** FT-IR spectra of the clay fractions (**a, a'**), the chitosan-clay films (**b, b'**), and the β- chitosan (**c, c'**). (**A**) and (**B**) are related to BN2 and RH, respectively. CM: clay minerals, Chit: chitosan, W: water, Q: quartz, S: silicates, St: stevensite.

(clay/chitosan mass ration: 1/1)

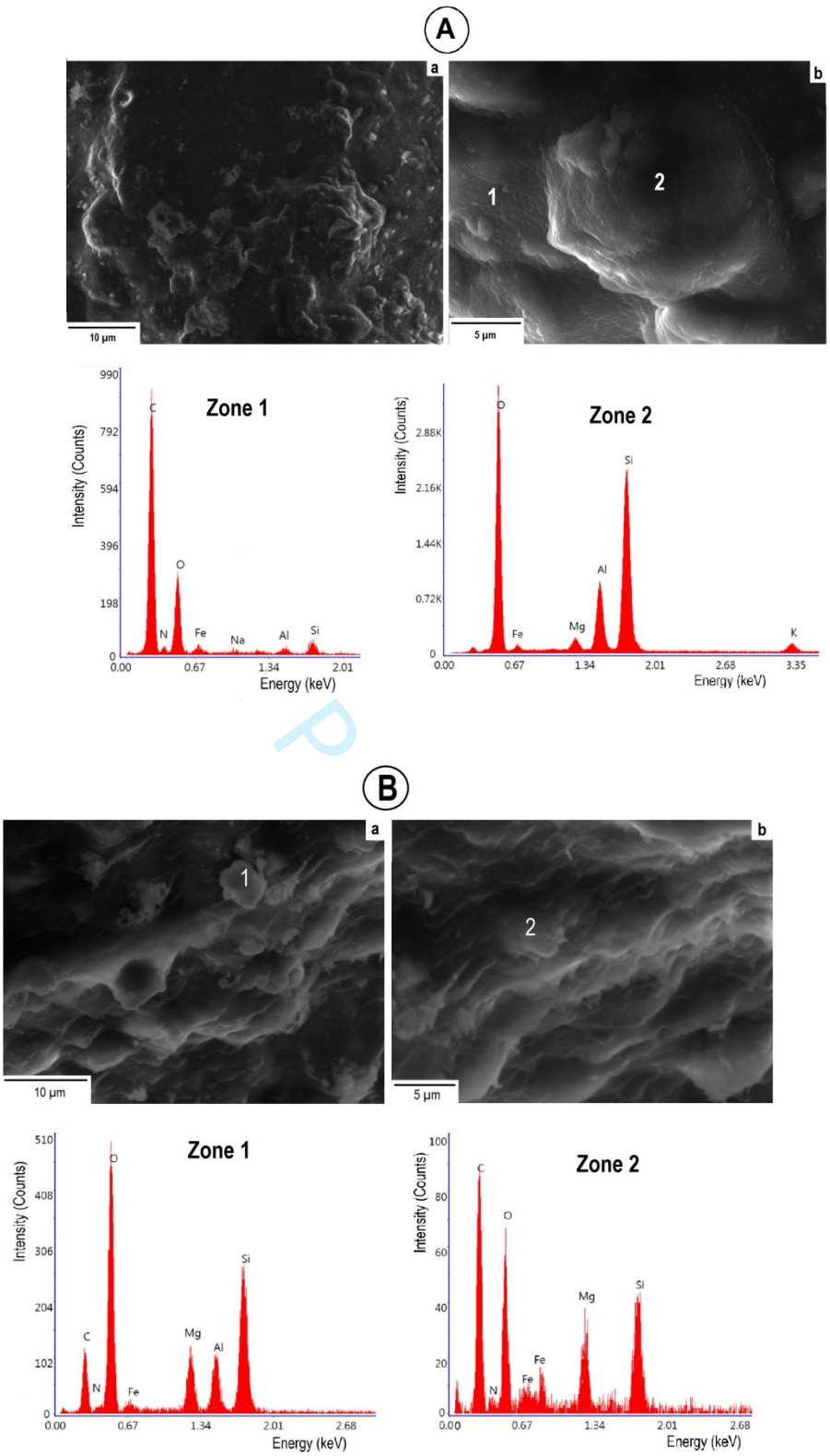


**Figure 5.** SEM micrographs of chitosan-BN2 (A) and chitosan-RH (B) films, and EDS spectra of different areas. Zone 1 (A) and zones 2 (B) are chitosan-rich domains. Zone 2 (A) and zone 1 (B) are clay-rich areas.

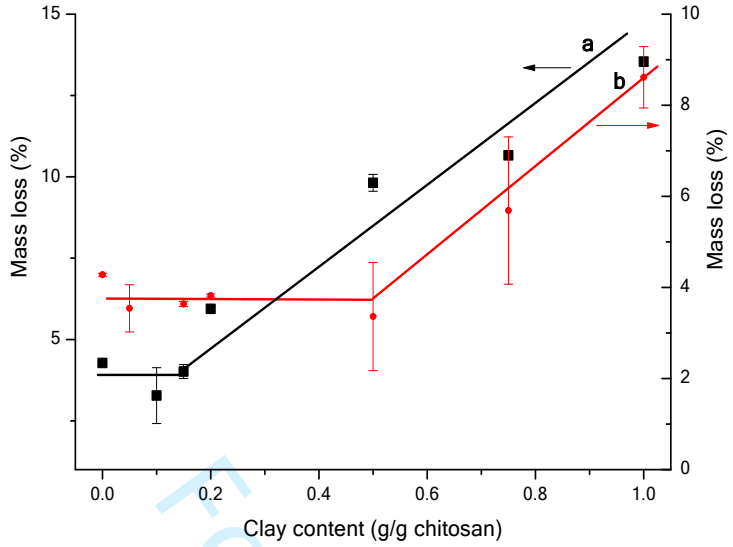


**Figure 6**. Variation of the mass loss of films vs. the clay content. (**a**) chitosan-RH film, (**b**) chitosan-BN2 film.

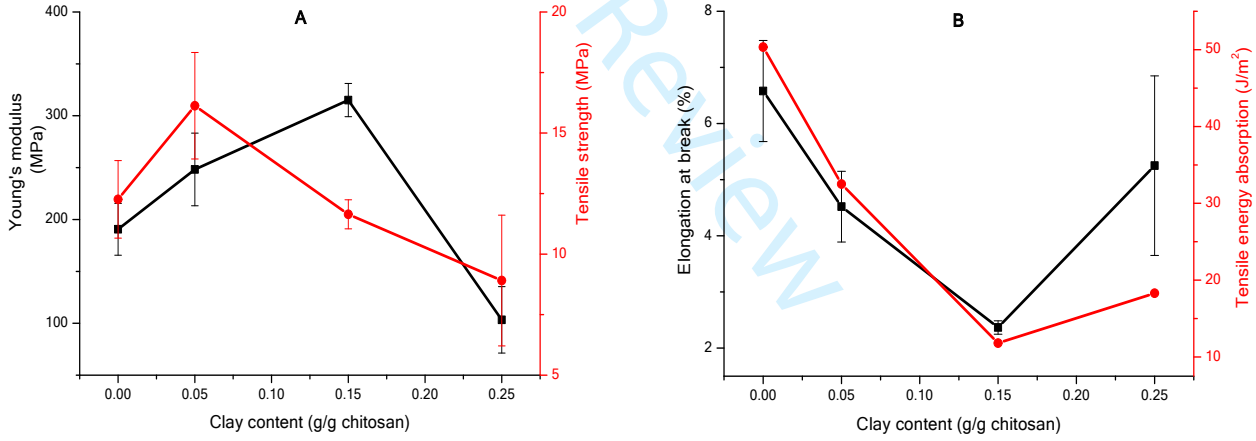


**Figure 7**. Variation of the mechanical properties of the chitosan-RH films as a function of the clay content. **A**: Young's modulus and tensile strength; **B**: Elongation at beak and tensile energy absorption.

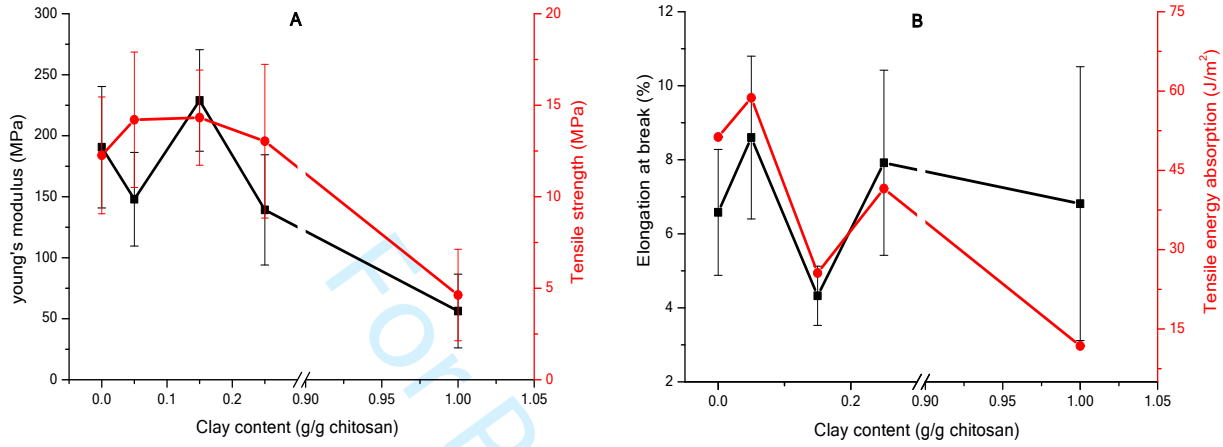


**Figure 8.** Evolution of the mechanical properties of the chitosan-BN2 films versus the clay content. **A**: Young's modulus and tensile strength; **B**: Elongation at beak and tensile energy absorption.

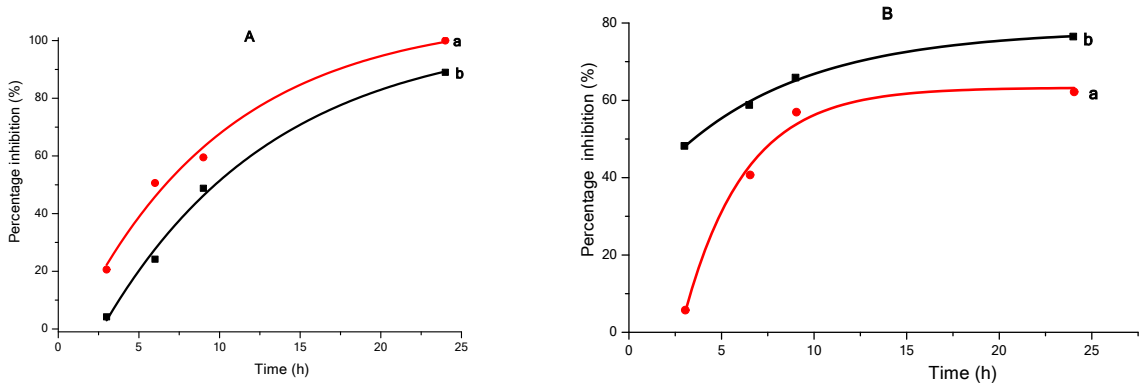


**Figure 9.** Kinetics curves associated to the inhibition growth of *E. coli* (**A**) and *S. aureus* (**B**) by the chitosan-RH (**a**) and the chitosan-BN2 (**b**) films.

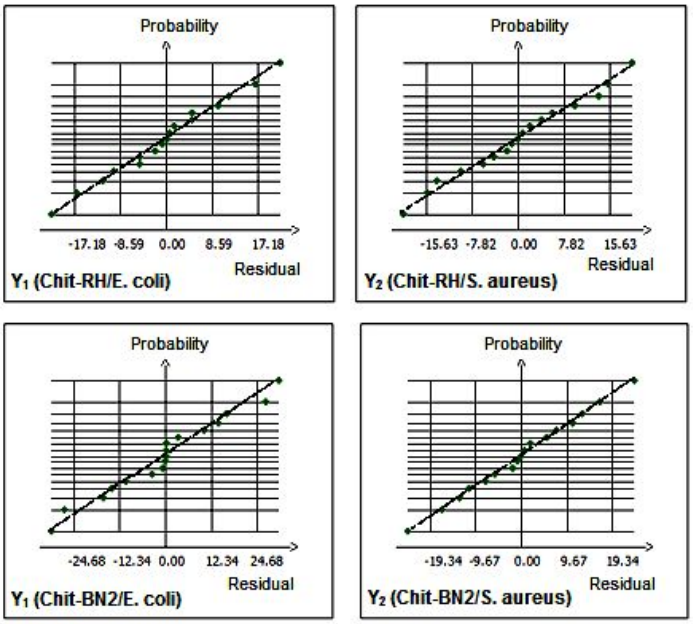


**Figure 10.** Probability plots of residuals related to the models used.

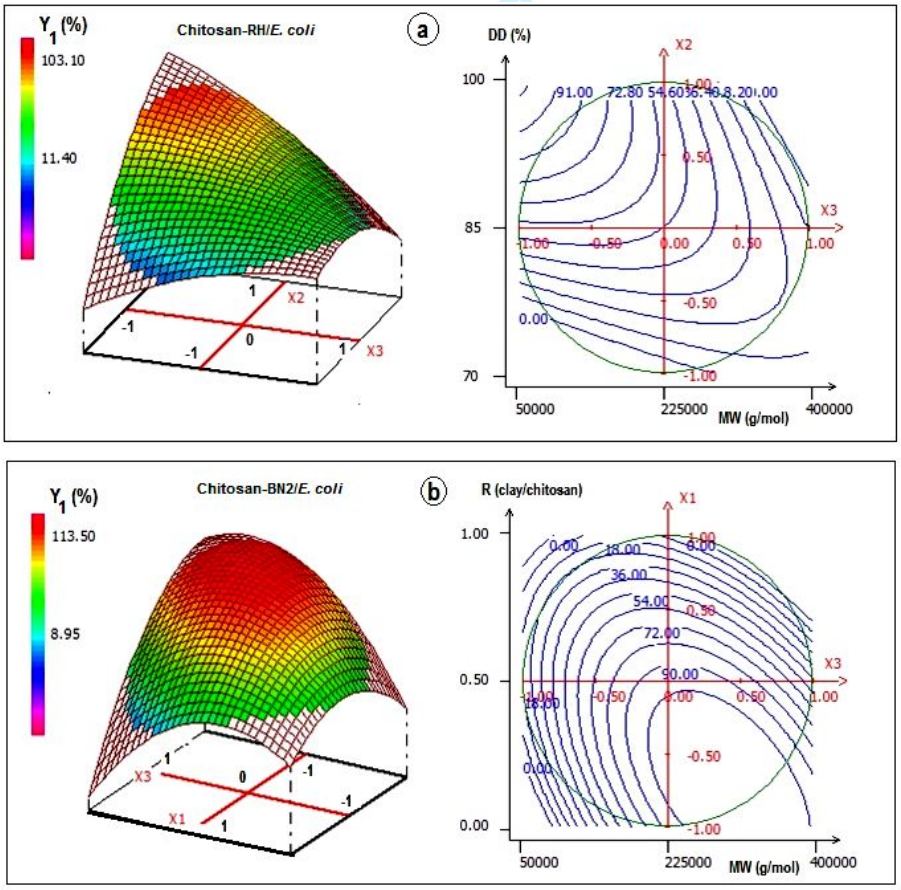

**Figure 11.** Variations of the percentage of inhibition of *E. coli* ($Y_1$ (Chitosan-RH), $Y_1$ (Chitosan-BN2)) against the factors studied. (**a**): clay/chitosan mass ratio (R) = 0.5; (**b**): deacetylation degree (DD) = 85%.

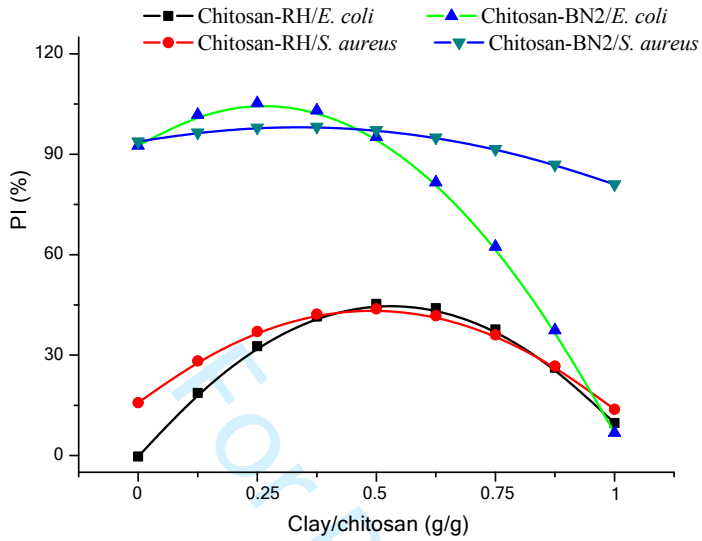


**Figure 12.** Variation of the percentage inhibition of the bacteria growth by the prepared films versus clay/chitosan mass ratio. DD = 85%, MW = 225000 g/mol.

**Table 1.** Chemical compositions (mass%) of the raw clays used, and $pH_{PZC}$ of the basic materials and the studied chitosan-clay films.

| **Chemical compositions** | | | | | | | |
|---|---|---|---|---|---|---|---|
| | $SiO_2$ | $Al_2O_3$ | $Fe_2O_3$ | MgO | CaO | $K_2O$ | $SO_3$ |
| BN2 | 48.1 | 16.5 | 7.3 | 4.5 | 19.4 | 2.8 | 1.4 |
| RH | 58.1 | 4.8 | 2.3 | 22.6 | 6.6 | 1.1 | 4.5 |

| **$pH_{PZC}$** | | | |
|---|---|---|---|
| Chitosan | BN2 | RH | Chitosan-clay films |
| 6.0 | 9.1 | 8.0 | 6.6 ± 0.3 |

**Table 2.** Experimental design matrix and the measured percentage inhibition ($Y_i$) of the bacteria (*E. coli* and *S. aureus*) by the films prepared.

| | | | | Chitosan-RH film | | Chitosan-BN2 film | |
|---|---|---|---|---|---|---|---|
| **Run** | **$X_1$** | **$X_2$** | **$X_3$** | **$Y_1$ (%)** | **$Y_2$ (%)** | **$Y_1$ (%)** | **$Y_2$ (%)** |
| | | | | ***E. coli*** | ***S. aureus*** | ***E. coli*** | ***S. aureus*** |
| 1 | 1.0000 | 0.0000 | 0.0000 | 0.00 | 0.00 | 0.00 | 75.36 |
| 2 | -1.0000 | 0.0000 | 0.0000 | 9.48 | 29.60 | 99.31 | 99.43 |
| 3 | 0.5000 | 0.8660 | 0.0000 | 62.93 | 80.17 | 96.54 | 87.68 |
| 4 | -0.5000 | -0.8660 | 0.0000 | 0.29 | 23.85 | 0.00 | 0.00 |
| 5 | 0.5000 | -0.8660 | 0.0000 | 0.00 | 0.00 | 0.00 | 0.00 |
| 6 | -0.5000 | 0.8660 | 0.0000 | 0.00 | 11.21 | 98.39 | 96.56 |
| 7 | 0.5000 | 0.2887 | 0.8165 | 0.00 | 0.00 | 0.00 | 94.56 |
| 8 | -0.5000 | -0.2887 | -0.8165 | 3.74 | 0.00 | 22.81 | 0.00 |
| 9 | 0.5000 | -0.2887 | -0.8165 | 19.83 | 5.75 | 35.71 | 6.02 |
| 10 | 0.0000 | 0.5774 | -0.8165 | 100.00 | 98.56 | 12.90 | 0.00 |
| 11 | -0.5000 | 0.2887 | 0.8165 | 19.54 | 0.00 | 95.62 | 94.84 |
| 12 | 0.0000 | -0.5774 | 0.8165 | 0.00 | 0.00 | 42.86 | 96.28 |
| 13 | 0.0000 | 0.0000 | 0.0000 | 44.64 | 44.64 | 94.47 | 99.14 |
| 14 | 0.0000 | 0.0000 | 0.0000 | 43.40 | 41.95 | 95.39 | 95.42 |
| 15 | 0.0000 | 0.0000 | 0.0000 | 45.48 | 42.82 | 95.39 | 97.99 |
| 16 | 0.0000 | 0.0000 | 0.0000 | 46.07 | 43.87 | 95.62 | 97.13 |
| 17 | 0.0000 | 0.0000 | 0.0000 | 46.98 | 45.98 | 95.16 | 96.56 |

**Table 3.** ANOVA results and statistical parameters related to the validity of the models adopted.

| | | Sources of variation | Sum of squares | Degrees of freedom | Mean square | F-ratio | Significance |
|---|---|---|---|---|---|---|---|
| Chitosan- RH film | $Y_1$ | Regression | 11555.4 | 9 | 1283.9 | 4.4 | <0.01 |
| | | Residues | 2046.3 | 7 | 292.3 | | |
| | | Total | 13601.7 | 16 | | | |
| | $Y_2$ | Regression | 12544.9 | 9 | 1393.9 | 5.1 | <0.01 |
| | | Residues | 1919.1 | 7 | 274.1 | | |
| | | Total | 14464.0 | 16 | | | |
| Chitosan-BN2 film | $Y_1$ | Regression | 27542.2 | 9 | 3060.2 | 11.9 | < 0.01 |
| | | Residues | 1793.1 | 7 | 256.2 | | |
| | | Total | 29335.3 | 16 | | | |
| | $Y_2$ | Regression | 28572.5 | 9 | 3174.7 | 8.9 | < 0.01 |
| | | Residues | 2499.4 | 7 | 357.1 | | |
| | | Total | 31071.9 | 16 | | | |

**Table 4.** Optimal operating factors for total inhibition of the bacteria growth determined by using the desirability function approach.

| | $X_1$ | R | $X_2$ | DD (%) | $X_3$ | MW (g/mol) |
|---|---|---|---|---|---|---|
| $Y_1$ (Chitosan-RH/*E. coli*) | 0.3554 | 0.68 | 0.6404 | 95 | -0.6808 | 105557 |
| $Y_2$ (Chitosan-RH/*S. aureus*) | 0.4572 | 0.73 | 0.7726 | 97 | -0.4405 | 147917 |
| $Y_1$ (Chitosan-BN2/*E. coli*) | -0.4861 | 0.26 | 0.6962 | 95 | 0.5282 | 317430 |
| $Y_2$ (Chitosan-BN2/*S. aureus*) | 0.6617 | 0.83 | 0.2956 | 89 | 0.6890 | 354370 |